Pergamon

Acta mater. Vol. 46, No. 13, pp. 4755–4768, 1998

Printed in Great Britain
PII: S1359-6454(98)00127-X
1359-6454/98 $19.00 + 0.00

THE THERMAL SHOCK RESISTANCE OF SOLIDS

T. J. LU† and N. A. FLECK
Cambridge University Engineering Department, Cambridge CB2 1PZ, U.K.

(Received 1 December 1997; accepted 28 March 1998)

Abstract—The thermal shock resistance of a brittle solid is analysed for an orthotropic plate suddenly exposed to a convective medium of different temperature. Two types of plate are considered: (i) a plate containing a distribution of flaws such as pores, for which a stress-based fracture criterion is appropriate, and (ii) a plate containing a single dominant crack aligned with the through-thickness direction, for which a critical stress intensity factor criterion is appropriate. First, the temperature and stress histories in the plate are given for the full range of Biot number. For the case of a cold shock, the stress field is tensile near the surface of the plate and gives rise to a mode I stress intensity factor for a pre-existing crack at the surface of the plate. Alternatively, for the case of hot shock, the stress field is tensile at the centre of the plate and gives rise to a mode I stress intensity factor for a pre-existing crack at the centre of the plate. Lower bound solutions are obtained for the maximum thermal shock that the plate can sustain without catastrophic failure according to the two distinct criteria: (i) maximum local tensile stress equals the tensile strength of the solid, and (ii) maximum stress intensity factor for the pre-existing representative crack equals the fracture toughness of the solid. Merit indices of material properties are deduced, and optimal materials are selected on the basis of these criteria, for the case of a high Biot number (high surface heat transfer) and a low Biot number (low surface heat transfer). The relative merit of candidate materials depends upon the magnitude of the Biot number, and upon the choice of failure criterion. The effect of porosity on thermal shock resistance is also explored: it is predicted that the presence of porosity is generally beneficial if the failure is dominated by a pre-existing crack. Finally, the analysis is used to develop merit indices for thermal fatigue. © *1998 Acta Metallurgica Inc. Published by Elsevier Science Ltd. All rights reserved.*

1. INTRODUCTION

A common measure of thermal shock resistance is the maximum jump in surface temperature which a brittle material can sustain without cracking. The subject is old and the literature large, yet existing theoretical models are not able to rank the shock resistance of materials in the observed manner. It is generally accepted that the thermal shock fracture resistance of a material depends on a number of material properties including the thermal expansion coefficient α, thermal conductivity k, thermal diffusivity κ, elastic modulus E, fracture toughness K_{IC}, tensile strength σ_f, and upon the additional parameters of heat transfer coefficient h, specimen size H, and duration of thermal shock (which is often overlooked).

A material with high fracture resistance under one set of thermal shock conditions may become deficient under other conditions. For instance, when quenched in air, BeO (beryllium oxide) exhibits much better shock resistance than aluminium oxide (Al_2O_3), but the order of merit switches when both materials are water quenched [1]. Additionally, experimental experience suggests that porosity is detrimental to the cold-shock resistance of ceramics but is beneficial to hot-shock resistance [2]. Current knowledge of the underlying mechanisms behind these phenomena appears to be rather limited.

A commonly used thermal shock parameter is the merit index of $\sigma_f/E\alpha$. This parameter only captures the *initiation* of thermal shock cracking in brittle materials under *extreme* conditions where the Biot number $Bi \equiv hH/k$ is infinite. An alternative thermal shock parameter, suggested by Hasselman [3], measures the ratio of the fracture energy for crack initiation to the fracture energy for continuous crack propagation. This parameter neglects the thermal conductivity of the material, a parameter considered central to thermal shock response. Other parameters for various geometries and thermal shock environments are also proposed [2, 4–10], and it appears that the details of the thermal fields must be coupled with material properties and geometrical parameters in order to successfully predict the fracture behaviour of a component subjected to thermal shock.

The present paper revisits the old problem of a plate of finite thickness, with faces suddenly exposed to a convective medium of different temperature. The main feature that differentiates this work from most previous studies (cf. for instance, Emery *et al.* [11], Nied [8], and Rizk and Radwan [9] who analyse the thermal shock fracture of an edge-cracked elastic plate) is that new non-

†To whom all correspondence should be addressed.

dimensional parameters capable of characterizing the thermal shock resistance of a brittle material are obtained in closed form over the full range of Biot number.

The paper begins by reviewing the transient temperature and stress distributions in a homogeneous orthotropic plate over the full range of Biot number, $Bi \equiv hH/k$. Closed-form expressions are obtained for the maximum stress, as well as its time of occurrence, attained at the surface and at the centre of the plate. Next, the fracture response of the plate is addressed, by assuming the plate contains a mode I crack extending perpendicular to the plate surface. For cold shock, the most damaging crack geometry is taken to be an edge crack, whereas for hot shock a centre-cracked plate is considered. It is reasonable to assume that the presence of these cracks has no effect on the one-dimensional temperature distribution within the plate. The mode I stress intensity factor for each crack geometry is calculated from the transient thermal stress field.

Two distinct failure criteria are considered for thermal shock resistance:

(i) A local tensile stress criterion, corresponding to the initiation of tensile fracture in a solid containing a distribution of flaws. For the sake of simplicity, the statistics of flaw distribution is neglected and it is assumed that the solid has a deterministic strength σ_f. Fracture occurs when the maximum tensile stress σ_{max} attains the strength σ_f.

(ii) A fracture toughness criterion, whereby the largest pre-existing flaw advances when the maximum stress intensity factor K_{max} attains the fracture toughness K_{IC}. It is assumed that this flaw is of the same length scale as the thickness of the structure. In most practical circumstances it will be demonstrated that this criterion is more restrictive than (i); this toughness criterion is, however, relevant to a ceramic component containing manufacturing flaws or service-induced flaws which scale with the size of the structure.

For each failure criterion, the maximum jump in surface temperature ΔT_{max} to withstand fracture is calculated for a single cold shock and for a single hot shock. The value of ΔT_{max} is sensitive to the magnitude of the surface heat transfer coefficient, via the Biot number Bi. Appropriate non-dimensional groups are identified that govern the thermal shock resistance of brittle solids over the full range of Biot number; these non-dimensional groups contain material, thermal and geometric parameters. The paper concludes with a discussion of the potential of porosity for increasing the thermal shock resistance of a solid, and on application of thermal shock analysis to thermal fatigue.

2. EVOLUTION OF TEMPERATURE AND STRESS

A crack-free infinite plate of thickness $2H$ is considered, with Cartesian coordinates embedded at the centre of the plate, as shown in Fig. 1. Initially, the plate is at a uniform temperature T_i, and at time $t = 0$ its top and bottom faces (at $z = \pm H$) are suddenly exposed to a convective medium of temperature T_∞.

Surface heat flow is assumed to satisfy

$$k_z \frac{\partial T}{\partial z} = \mp h(T_\infty - T), \text{ at } z = \pm H \tag{1}$$

where k_z is the thermal conductivity of the solid in the z-direction, h the coefficient of heat transfer, and $T(z,t)$ the temperature of the solid. Heat flow within the solid induces a transient temperature distribution $T(z,t)$ and a stress state $\sigma(z,t)$. The plate is assumed to comprise a uniform, linear thermo-elastic solid with axes of orthotropy aligned with the Cartesian coordinates (x,y,z) given in Fig. 1. The strain state ε is given by

$$\varepsilon_{xx} = \frac{1}{E_x}\sigma_{xx} - \frac{\nu_{xy}}{E_y}\sigma_{yy} - \frac{\nu_{xz}}{E_z}\sigma_{zz} + \alpha_x(T - T_i) \tag{2a}$$

$$\varepsilon_{yy} = -\frac{\nu_{xy}}{E_y}\sigma_{xx} + \frac{1}{E_y}\sigma_{yy} - \frac{\nu_{yz}}{E_z}\sigma_{zz} + \alpha_y(T - T_i) \tag{2b}$$

$$\varepsilon_{zz} = -\frac{\nu_{xz}}{E_z}\sigma_{xx} - \frac{\nu_{yz}}{E_z}\sigma_{yy} + \frac{1}{E_z}\sigma_{zz} + \alpha_z(T - T_i). \tag{2c}$$

Here, (E_x,E_y,E_z) are the elastic moduli in the (x,y,z) directions, respectively, $(\nu_{xy},\nu_{xz},\nu_{yz})$ the Poisson ratios, and $(\alpha_x,\alpha_y,\alpha_z)$ the coefficients of thermal expansion. Symmetry dictates that the shear stress and shear strain components vanish.

The configuration in Fig. 1 is analysed under the constraint that the plate is free to expand with vanishing axial force

$$\int_{-H}^{H} \sigma_{xx}\, dz = 0$$

and

$$\int_{-H}^{H} \sigma_{yy}\, dz = 0$$

and vanishing normal stress in the through-thick-

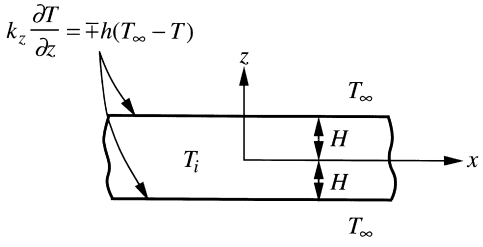

Fig. 1. A finite-thickness plate suddenly exposed to a convective medium of different temperature.

ness direction $\sigma_{zz} = 0$. The geometry and boundary conditions are such that the strain ε is independent of all spatial dimensions including z, and depends only on time t: the plate stretches uniformly but does not bend.

It follows from equations (2) that the transient thermally-induced stress $\sigma_{xx}(z,t)$ associated with the temperature distribution $T(z,t)$ is

$$\sigma_{xx}(z,t) = -\bar{E}\bar{\alpha}(T - T_i) + \frac{\bar{E}\bar{\alpha}}{2H}\int_{-H}^{H}(T - T_i)\,dz \quad (3a)$$

where

$$\bar{E} \equiv \frac{1}{E_x} - \frac{\nu_{xy}^2}{E_y}, \text{ and } \bar{\alpha} \equiv \alpha_x + \nu_{xy}\alpha_y \quad (3b)$$

The two elastic parameters, $\bar{E}$ and $\bar{\alpha}$, are extensively used in this paper. A parallel relation exists for the thermal stress $\sigma_{yy}(z,t)$, and can be found directly from equation (3a) upon rotating the plate by 90° about the z-axis. Here, it is assumed without loss of generality that the stress component initiating fracture is $\sigma_{xx}(z,t)$ and attention is restricted to this stress component only.

2.1. Temperature distribution

Heat flow in the through-thickness direction for the orthotropic plate shown in Fig. 1 is governed by

$$\frac{\partial^2 T}{\partial z^2} = \frac{1}{\kappa_z}\frac{\partial T}{\partial t}, \quad |z| \le H \quad (4a)$$

where κ_z is the thermal diffusivity of the solid in the z-direction. Upon introducing the dimensionless spatial variable $\bar{z} = z/H$ and dimensionless time $\bar{t} = \kappa_z t/H^2$, equation (4a) simplifies to

$$\frac{\partial^2 T}{\partial \bar{z}^2} = \frac{\partial T}{\partial \bar{t}}, \quad |\bar{z}| \le 1. \quad (4b)$$

It can be seen immediately that the thermal diffusivity κ_z dictates the time-scale for the transient stress state within the plate, but does not affect the level of thermal stresses. Equation (4) is solved with heat transfer boundary condition (1) by a standard separation-of-variables technique [12], giving

$$\frac{T(z,t) - T_i}{T_i - T_\infty} = -1 + 2\sum_{n=1}^{\infty}\exp\left(-\beta_n^2\frac{\kappa_z t}{H^2}\right) \times \frac{\sin\beta_n \cos(\beta_n z/H)}{\beta_n + \sin\beta_n\cos\beta_n} \quad (5)$$

where β_n are the roots of

$$\beta_n \tan\beta_n = Bi \quad (6)$$

and the non-dimensional heat transfer coefficient $Bi = hH/k_z$ is the Biot number for the orthotropic solid. In the limit of perfect thermal insulation $Bi = 0$, $\beta_n = n\pi$ and $T(z,t) \equiv T_i$. At the other limit of perfect heat transfer, $Bi = \infty$, $\beta_n = (n + 1/2)\pi$ and equation (5) simplifies to

$$\frac{T(z,t) - T_i}{T_i - T_\infty} = -1 + \frac{4}{\pi}\sum_{n=0}^{\infty}\frac{(-1)^n}{2n+1} \times \exp\left(-\frac{(2n+1)^2\pi^2}{4}\frac{\kappa_z t}{H^2}\right) \times \cos\left[\frac{(2n+1)\pi}{2}\frac{z}{H}\right]. \quad (7a)$$

For finite values of Bi, the coefficient β_n is determined numerically and is bounded by the two limiting values given above

$$n\pi < \beta_n < (n + 1/2)\pi, \quad n = 0,1,2,\ldots \quad (7b)$$

2.2. Transient stress distribution

The thermal stress $\sigma(z,t) \equiv \sigma_{xx}(z,t)$ is obtained directly from equations (3a) and (5), and is written in non-dimensional form as

$$\bar{\sigma} \equiv \frac{\sigma(z,t)}{\bar{E}\bar{\alpha}(T_i - T_\infty)} = \frac{T(z,t) - T_i}{T_i - T_\infty} - \frac{1}{2H}\int_{-H}^{H}\frac{T(z,t) - T_i}{T_i - T_\infty}dz = 2\sum_{n=1}^{\infty}\exp\left(-\beta_n^2\frac{\kappa_z t}{H^2}\right)\frac{\sin\beta_n}{\beta_n + \sin\beta_n\cos\beta_n} \times \left\{\cos\left(\beta_n\frac{z}{H}\right) - \frac{\sin\beta_n}{\beta_n}\right\}. \quad (8)$$

In the limit $Bi = 0$, the plate is everywhere stress free (i.e. $\sigma(z,t) \equiv 0$) while, if $Bi = \infty$

$$\bar{\sigma} \equiv \frac{\sigma(z,t)}{\bar{E}\bar{\alpha}(T_i - T_\infty)} = \frac{4}{\pi}\sum_{n=0}^{\infty}\exp\left(-\frac{(2n+1)^2\pi^2}{4}\frac{\kappa_z t}{H^2}\right) \times \left\{\frac{(-1)^n}{2n+1}\cos\left[\frac{(2n+1)\pi}{2}\frac{z}{H}\right] - \frac{2}{(2n+1)^2\pi}\right\}. \quad (9)$$

When Bi is small ($Bi < 2$), it has been established that the stress distribution is dominated by the first two terms of equation (8).

The evolution of dimensionless stress, $\bar{\sigma}(z,t) \equiv \sigma(z,t)/\bar{E}\bar{\alpha}(T_i - T_\infty)$, is plotted against dimensionless time, $\bar{t} \equiv \kappa_z t/H^2$ in Fig. 2, at selected locations through the thickness of the plate, $\bar{z} \equiv z/H$ and for $Bi = \infty$, 10 and 1. Under cold shock conditions ($T_i > T_\infty$), the surface layers experience a tensile stress transient while a compressive zone is developed at the centre of the plate. For all values of Bi, the maximum tensile stress is attained at the surface and the compressive stress is largest at the centre of the plate. The overall magnitude of the stresses increases with increasing Bi.

The transient tensile stress at the surface explains the common observation that, during cold shock, a crack initiates at the surface and grows unstably until it enters the central compressive region. Alternatively, during a hot shock event ($T_\infty > T_i$)

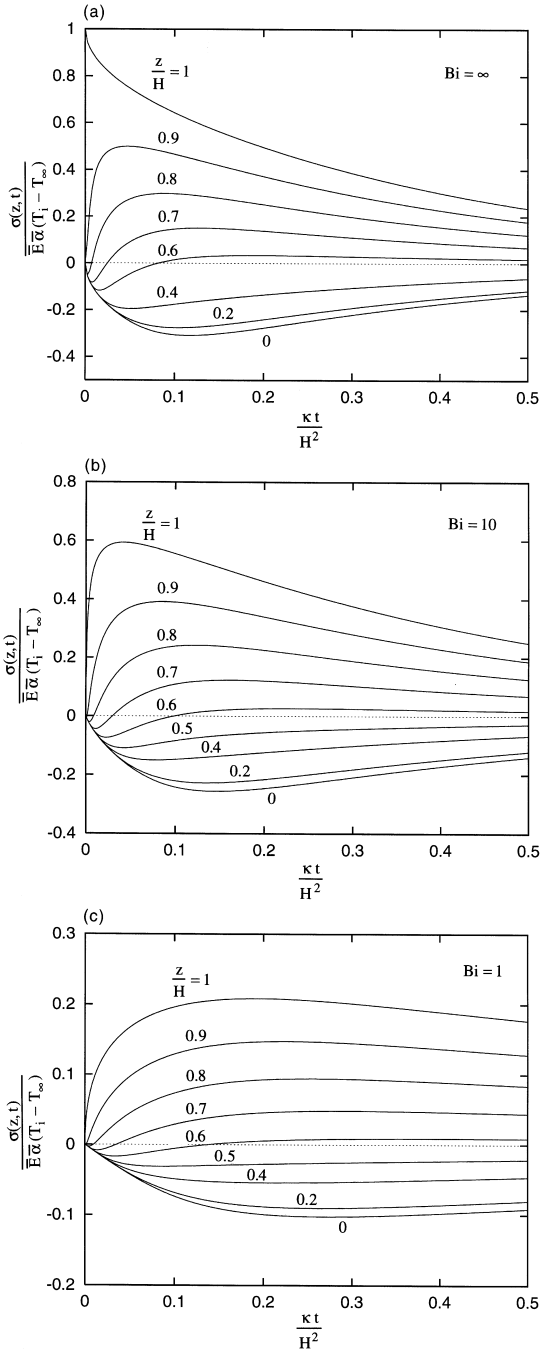

Fig. 2. Evolution of dimensionless stress $\bar{\sigma}(z,t)$ as a function of dimensionless time $\bar{t}$ at selected locations z/H for: (a) $Bi = \infty$; (b) $Bi = 10$; (c) $Bi = 1$.

the centre of the plate is under tension and is prone to cracking; spalling of a surface layer due to large compressive stress is also a possibility [2, 5]. This study will focus on failure due to tensile stress at the surface of the plate in cold shock, and at the centre of the plate in hot shock. (Notice that an edge crack may also grow under hot shock if the crack is sufficiently long [13], but this scenario is not considered in the analysis presented below.) It is convenient to change the sign in the definition of $\bar{\sigma}$ for hot shock: from now on, $\bar{\sigma}$ is re-defined for hot shock as $\bar{\sigma}(z,t) \equiv \sigma(z,t)/\bar{E}\bar{\alpha}(T_\infty - T_i)$ so that both $\bar{\sigma}$ and σ are positive at the centre of the plate.

The transient tensile stress at the surface of the plate in cold shock, and at the centre of the plate in hot shock, is plotted in Figs 3(a) and (b), respectively, for selected values of Bi. For the limiting case of an ideal cold shock ($Bi = \infty$), a maximum value of $\bar{\sigma} = 1$ is achieved at the surface of the plate at $\bar{t} = 0$. For an ideal hot shock ($Bi = \infty$), the maximum tensile stress achieved at the plate centre is $\bar{\sigma}_{\max} = 0.3085$ at a time $\bar{t}^* = 0.115$ by equation (9).

The maximum tensile stress $\bar{\sigma}_{\max}$ achieved at the surface during cold shock is plotted against $1/Bi$ in Fig. 3(c); for comparison purposes, the maximum tensile stress at the centre of the plate during hot shock is included in the figure. It is clear that the magnitude of $\bar{\sigma}_{\max}$ increases with increasing Bi for both hot shock and cold shock. Further, the magnitude of $\bar{\sigma}_{\max}$ is always less for hot shock than for cold shock, at any give value of Bi. The maximum surface stress in cold shock is adequately described by the relation

$$\bar{\sigma}_{\max}(\pm H, t^*) = \left\{1.5 + \frac{3.25}{Bi} - 0.5e^{-16/Bi}\right\}^{-1} \quad (10a)$$

whereas, to an excellent approximation, the maximum stress developed at the centre in hot shock is given by

$$\bar{\sigma}_{\max}(0, t^*) = \frac{0.3085}{1 + (2/Bi)} \quad (10b)$$

as shown by the comparison in Fig. 3(c). The semi-empirical equation (10a) was suggested by Manson [14], based on an earlier result of Buessem [15]; this relation has subsequently been widely used, together with the maximum tensile-stress criterion, to calculate the resistance of both brittle and ductile materials to crack initiation under cold shock conditions [1, 4, 5].

For completeness, the time of occurrence of $\bar{\sigma}_{\max}$ at the surface during cold shock and at the centre during hot shock is plotted against $1/Bi$ in Fig. 3(d). The time t^* needed for the surface layer to reach the maximum stress in cold shock is given approximately by

$$\bar{t}^* = \kappa_z t^*/H^2 = \frac{0.48}{1 + 1.8Bi}. \quad (11a)$$

Similarly, the time for the centre of the plate to attain the maximum tensile stress under hot shock is approximated by

$$\bar{t}^* = \kappa_z t^*/H^2 = 0.115 + \frac{0.45}{1 + 2.25Bi}. \quad (11b)$$

equations (11a) and (b) describe closely the time dependence of maximum thermal stress at the sur-

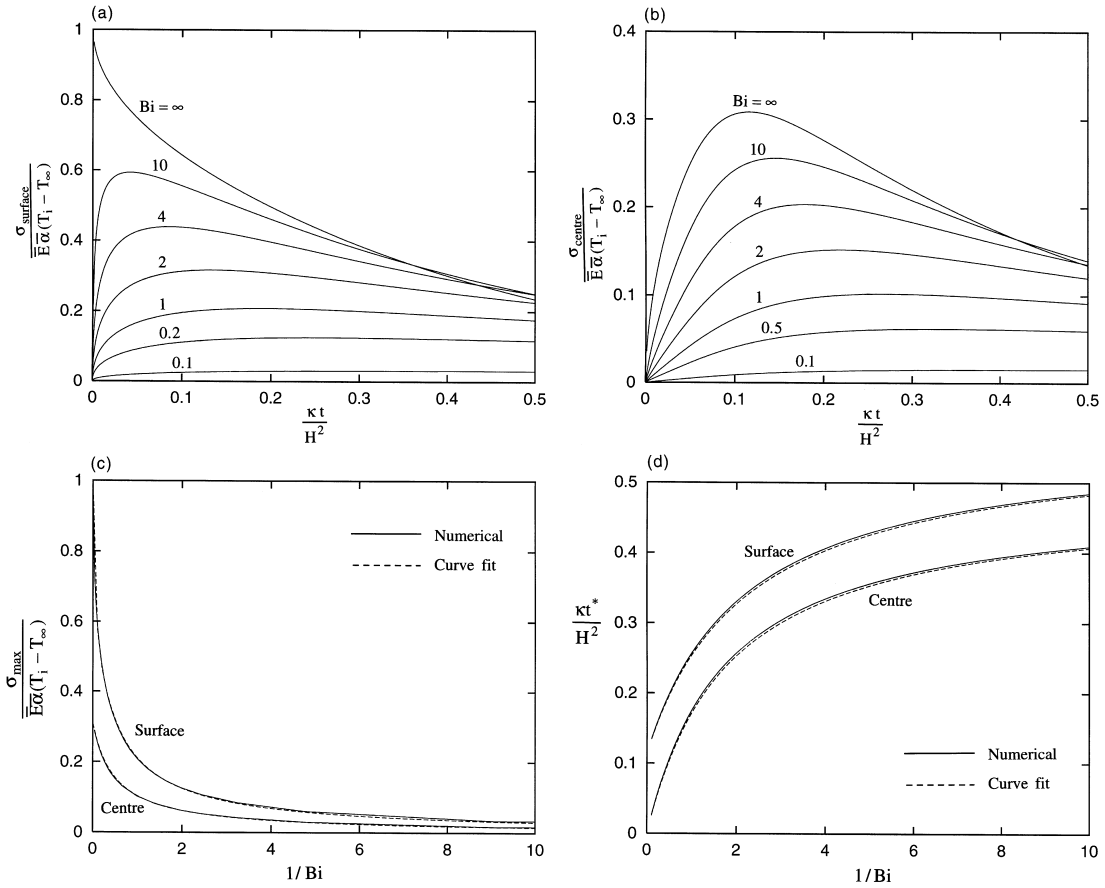

Fig. 3. (a) Surface stress $\bar{\sigma}_{\text{surface}}$ in cold shock and (b) centre stress $\bar{\sigma}_{\text{centre}}$ in hot shock as a function of time $\bar{t}$ for selected values of Biot number, Bi; (c) maximum surface stress and maximum centre stress, $\bar{\sigma}_{\max}$, and (d) their time of occurrence, $\bar{t}^*$, as functions of $1/Bi$. The dashed lines in (c) and (d) represent the empirical relations (10) and (11).

face and at the centre, respectively, as shown by the comparison in Fig. 3(d). So far a maximum tensile stress criterion for fracture initiation has been discussed. In the case of a structure containing defects on the order of the structural dimension it is more appropriate to determine the temperature jump for which a pre-existing crack will grow.

3. CRACKING DUE TO COLD SHOCK

Consider again the infinite plate of Fig. 1 subjected to a cold shock. If the plate contains a number of large cracks on the scale of the plate thickness then it is expected that cracking will commence from the "worst flaw". A rational definition of "worst flaw" is the one which has the largest transient mode I stress intensity factor. The problem is idealized to the highly simplified case of a plate containing an isolated mode I edge crack of depth a, as shown in Fig. 4(a). For this crack the stress intensity factor K is calculated during a cold shock event, for $0 < Bi \leq \infty$. Since the crack plane is normal to the face of the plate, it does not perturb the transient temperature distribution. The stress intensity factor K associated with the thermal stress $\sigma(z,t)$ is derived by straightforward numerical integration making use of the appropriate weight function, to give

$$\frac{K}{K^0} = \frac{\lambda^{-3/8}}{\sqrt{n}} \frac{2}{\pi\sqrt{a/H}} \int_{1-a/H}^{1} \times \left[\frac{F_1(z/H,a/H)\bar{\sigma}(z/H,t)}{(1-a/2H)^{1.5}\sqrt{1-[(H-z)/a]^2}} \right] \mathrm{d}\left(\frac{z}{H}\right). \tag{12}$$

Here, $K^0 \equiv \sqrt{\pi H}\bar{E}\bar{\alpha}(T_i - T_\infty)$ is a reference stress intensity factor, and $F_1(z/H,a/H)$ is a non-dimensional function defined in equation (A1) of Appendix A. The concept of orthotropic rescaling [16] has been used to account for material anisotropy. With the aid of the orthotropic stress–strain relation (2), the two non-dimensional elastic parameters λ, n are defined as

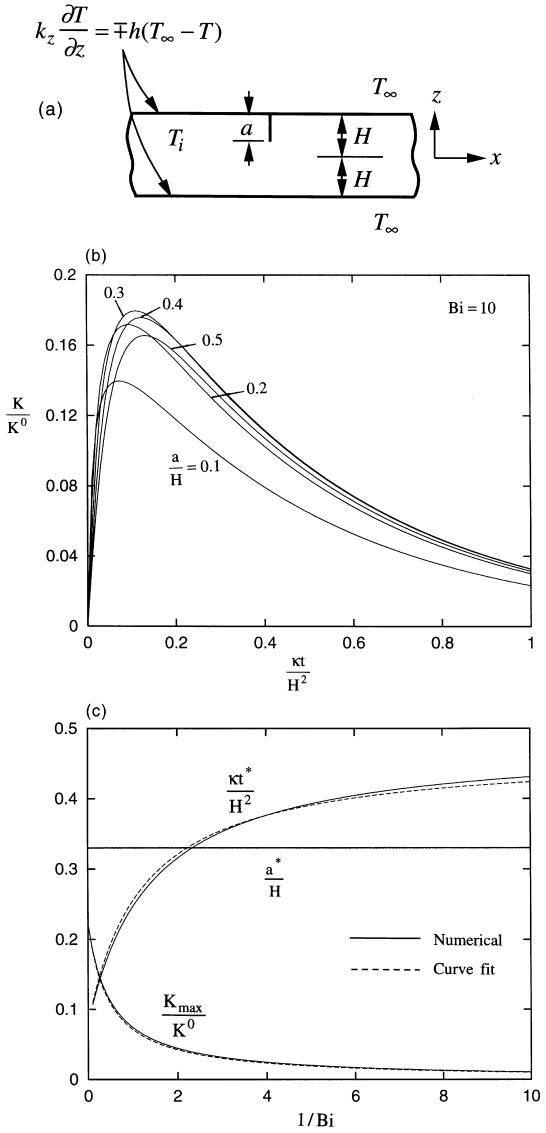

Fig. 4. (a) Geometry and conventions for a single edge crack under cold shock, (b) dimensionless stress intensity factor $\bar{K}$ as a function of dimensionless time $\bar{t}$ for $Bi = 10$, (c) $\bar{K}_{max}$ and the corresponding non-dimensional values $\bar{t}^*$ and $\bar{a}^*$ plotted as functions of $1/Bi$. The dashed lines in (c) and (d) represent the empirical relations (14).

$$\lambda = \frac{\bar{E}_z}{\bar{E}_x},\ n = \sqrt{\frac{1+\zeta}{2}} \text{ where}$$

$$\zeta = \frac{\sqrt{\bar{E}_x \bar{E}_z}}{2G_{xz}} \left\{ 1 - 2\nu_{xz} \frac{G_{xz}}{E_z} \left(1 - \frac{E_z}{E_y} \frac{\nu_{xy}\nu_{yz}}{\nu_{xz}} \right) \right\} \qquad (13)$$

and $\bar{E}_x \equiv \bar{E}$, $\bar{E}_z \equiv (1/E_z - \nu_{zy}^2/E_y)^{-1}$. The shear modulus in the x–z plane is denoted by G_{xz}. Positive definiteness of the strain energy density requires $\lambda > 0$ and $-1 < \zeta < \infty$. For the sake of brevity only the case of a transversely isotropic solid will be considered for which the material is isotropic in planes normal to the y-axis and $\lambda = \zeta = 1$.

The normalized stress intensity factor $\bar{K} \equiv K/K^0 = K/\sqrt{\pi H}\bar{E}\bar{\alpha}(T_i - T_\infty)$ is plotted against dimensionless time $\bar{t} \equiv \kappa_z t/H^2$ in Fig. 4(b), for selected normalized crack length $\bar{a} \equiv a/H$. For illustrative purposes, results are presented only for the case $Bi = 10$; results over the full range of Biot number ($0 < Bi \leq \infty$) are qualitatively similar to those shown. At any given crack length a, K displays a peak value after a finite time and decreases to zero as $t \to 0$ and as $t \to \infty$. It is further noted that the magnitude of K depends upon crack length, and achieves a peak value for a crack of length $a/H \approx 1/3$. Thus, for a given Biot number Bi, K achieves a global maximum value K_{max} at a time t^* and at a crack length a^*. Non-dimensional values of K_{max} and the corresponding non-dimensional values $\bar{t}^* \equiv t\kappa_z/H^2$ and $\bar{a}^* \equiv a^*/H$ are plotted in Fig. 4(c) as a function of $1/Bi$. Simple curve fits to the plots of K_{max} and $(\bar{t}^*, \bar{a}^*)$ against $1/Bi$ are given by

$$\bar{K}_{max} \equiv \frac{K_{max}}{K^0} = 0.222\left(1 + \frac{2.12}{Bi}\right)^{-1} \qquad (14a)$$

$$\bar{t}^* \equiv \frac{\kappa t^*}{H^2} = 0.08 + \frac{0.4}{1 + 1.4Bi} \qquad (14b)$$

$$\bar{a}^* \equiv \frac{a^*}{H} = \frac{1}{3} \qquad (14c)$$

and are in satisfactory agreement with the precise values. It is clear from Fig. 4(c), and from equations (14) that K attains its maximum value approximately at $a/H = 1/3$ and $\kappa t^*/H^2 = 0.1$, for $Bi > 5$. It is important to note that the limiting value $K_{max} = 0.222K^0$ is the largest stress intensity factor attained for any crack length, under the most severe thermal shock boundary condition ($Bi = \infty$). This limit also applies to an edge crack under hot shock [13] and a centre crack under hot shock (see the results in the next section).

For the purposes of material selection for cold shock, it is assumed the plate contains a "worst flaw": this flaw is taken as an edge crack of length $a^* = H/3$ which maximizes K during the cold shock. Assume that failure occurs when K_{max} given by equation (14a) equals K_{IC} for the solid. The subsequent path of propagation of the edge crack remains to be discussed. After propagating straight-ahead towards the centre of the plate, the crack increasingly feels the presence of compressive stresses in the central portion of the plate and K drops. As soon as the crack enters the central portion of the plate under compression, the T-stress at the crack tip changes from negative to positive [17] which, according to Cotterell and Rice [18], causes the straight-ahead advance of the crack to become configurationally unstable. More specifically, in the

presence of a positive T-stress, the crack may deflect parallel to the surface, resulting in crack branching or spalling. Deflection is encouraged by compressive residual stresses in ceramic laminates (and by other crack deflectors such as pores and weak interfaces); this has been the subject of several recent studies [16, 17, 19, 20]. Development of these concepts is left to a later study.

4. CRACKING DUE TO HOT SHOCK

Now consider the plate of Fig. 1 subjected to a hot shock: initially the plate is at a uniform temperature T_i. At time $t = 0$ the top and bottom surface of the plate are exposed to an environment at temperature $T_\infty (> T_i)$, and the surface heat transfer condition is again given by equation (1). As discussed above, the hot shock induces transient tensile stresses at the centre of the plate, with peak value specified by equation (10b).

A plate under hot shock is most likely to develop mode I cracks in the centre of the plate where maximum tensile stress is attained. In order to develop a thermal shock criterion, the magnitude of hot shock required to propagate a pre-existing centre crack of length $2a$, symmetrical with respect to $z = 0$ is determined [Fig. 5(a)]. The mode I stress intensity factor associated with the thermal stress transient (9) is given by integration of $\sigma(z,t)$ over the crack face, with respect to the appropriate weight function

$$\frac{K}{K^0} = \frac{\lambda^{-3/8}}{\sqrt{n}} \sqrt{\frac{2}{\pi} \tan \frac{\pi a}{2H}} \times \int_0^{a/H} \left[\frac{F_2(z/H, a/H)\bar{\sigma}(z/H, t)}{\sqrt{1 - \left(\cos \frac{\pi a}{2H} \cos \frac{\pi}{2} \frac{z}{H} \right)^2}} \right] \mathrm{d}\left(\frac{z}{H} \right). \quad (15)$$

The dimensionless function $F_2(z/H, a/H)$ is given by equation (A2) of Appendix A. Note that under hot shock, the parameter K^0 is defined by $K^0 = \sqrt{\pi H} \bar{E} \bar{\alpha} (T_\infty - T_i)$ since $T_\infty > T_i$. For brevity, again attention is restricted to transversely isotropic plates ($\lambda = \zeta = 1$).

The non-dimensional stress intensity factor K/K^0 is evaluated by numerical integration of equation (15), and is plotted against time in Fig. 5(b), for selected values of crack length and for the particular choice $Bi = 10$. The qualitative shape of the response is similar for other Biot numbers: K increases from zero to a maximum value, and then decays back to zero. It can be noted from Fig. 5(b) that K attains an overall maximum value $K_{\max}$ at a particular time t^* and at a particular crack length $2a^*$. The values of $(K_{\max}, t^*, a^*)$ depend upon the Biot number, as shown in Fig. 5(c).

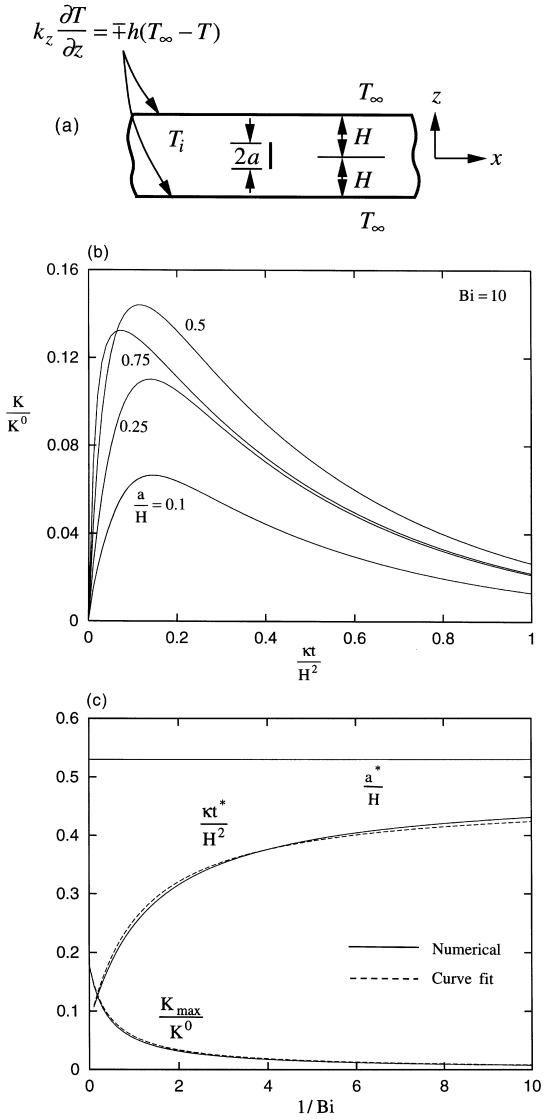

Fig. 5. (a) Geometry and conventions for a centre crack under hot shock, (b) dimensionless stress intensity factor $\bar{K}$ as a function of dimensionless time $\bar{t}$ for $Bi = 10$, (c) $\bar{K}_{\max}$, and the corresponding non-dimensional values $\bar{t}^*$ and $\bar{a}^*$ plotted as functions of $1/Bi$. The dashed lines in (c) and (d) represent the empirical relations (16).

As expected, $K_{\max}$ achieves a peak value ($\bar{K}_{\max} \equiv K_{\max}/K^0 = 0.177$) for the case of perfect heat transfer $Bi = \infty$. With decreasing Bi, $K_{\max}$ decreases in a monotonic manner. A curve fit to the plot of $\bar{K}_{\max} \equiv K_{\max}/K^0$ vs $1/Bi$ is included in Fig. 5(c), and is adequately approximated by

$$\bar{K}_{\max} = 0.177 \left(1 + \frac{2.12}{Bi} \right)^{-1}. \quad (16a)$$

For the full range of Biot number ($0 < Bi \leq \infty$) K is largest for a crack length of approximately $a/H = 0.5$. Accurate curve fits for (t^*, a^*) are

included in Fig. 5(c), and are given by

$$\bar{t}^* = \frac{\kappa t^*}{H^2} = 0.08 + \frac{0.4}{1 + 1.4Bi} \tag{16b}$$

$$\bar{a}^* \equiv \frac{a^*}{H} = 0.5 \tag{16c}$$

In order to select a material of optimal thermal shock resistance, the plate containing a centre crack of length $2a^*$ is considered such that K is maximized during the hot shock. Assume that failure occurs when $K_{\max}$ given by equation (16a) equals K_{IC} for the solid. It is clear from a comparison of equations (14a) and (16a), and from a comparison of equations (10a) and (b) that the hot shock resistance for a centre-cracked plate is greater than the cold shock resistance for an edge-cracked plate, regardless of whether failure is strength-controlled or toughness-controlled. In the latter case, this is true for all values of Bi, as long as the crack length does not exceed a critical length a_{critical} where the stress intensity factor under cold shock equals that under hot shock. For an edge-cracked plate having $a > a_{\text{critical}}$, a hot shock then becomes more severe than a cold shock [13]. Also, as K increases continuously with increases in a for an edge crack under hot shock, crack propagation is inherently unstable; under cold shock, crack extension is stable once the crack length reaches a^* thereafter $\mathrm{d}K/\mathrm{d}a<0$ [cf. Fig. 4(b)]. For a finite plate with two symmetrical edge cracks subjected to severe thermal shock $Bi = \infty$, it has been found that $a_{\text{critical}} = 0.6H$ [13].

5. THERMAL SHOCK MATERIAL PARAMETERS FOR ENGINEERING CERAMICS

Thermal shock resistance is a major issue in the selection of engineering ceramics for thermal applications, such as furnaces and engine parts. A central problem in designing against thermal shock is the identification of appropriate material selection criteria in order to select the most shock resistant material for a given application. Material performance indices are summarized for both strength-controlled failure and toughness-controlled failure.

5.1. Merit indices for strength-controlled failure

A stress-based fracture criterion for cold shock is that $\sigma_{\max}(\pm H, t^*)$ attains the fracture strength of the solid σ_f; similarly, for hot shock $\sigma_{\max}(0, t^*)$ attains the value σ_f. The maximum temperature jump sustainable by the solid ΔT in the extreme case of perfect heat transfer ($Bi = \infty$) follows from equations (10a) and (b) as

$$\Delta T = A_1 \frac{\sigma_f}{E\alpha} \tag{17}$$

where $A_1 \approx 1$ for cold shock, and $A_1 \approx 3.2$ for hot shock. Here, and in the following, the distinction between E and $\bar{E}$, and between α and $\bar{\alpha}$ has been dropped, as broad material selection criteria are concerned with, and terms of minor significance are neglected. The temperature jump sustainable increases with decreasing Biot number, so that in the limit of small Biot number ($Bi < 1$), ΔT follows from equations (10a) and (b) as

$$\Delta T = A_2 \frac{\sigma_f}{E\alpha} \frac{1}{Bi} \equiv A_2 \frac{\sigma_f}{E\alpha} \frac{k}{hH} \tag{18}$$

where $A_2 \approx 3.2$ for cold shock, and $A_2 \approx 6.5$ for hot shock. It is clear from equation (17) that for perfect heat transfer the highest temperature jumps are achieved for materials with a large value of $\sigma_f/E\alpha$. In the case of poor surface heat transfer ($Bi < 1$), the best materials have the largest value of the material property group $k\sigma_f/E\alpha$.

It is instructive to map engineering ceramics on a plot with axes $k\sigma_f/E\alpha$ and $\sigma_f/E\alpha$, as shown in Fig. 6(a). The Cambridge Materials Selector software [21] is particularly useful for this purpose. Materials of high thermal shock resistance under conditions of ideal heat transfer lie to the right of the diagram, and materials of high thermal shock resistance under conditions of poor heat transfer lie to the top of the diagram. Glass ceramics and graphites lie at the extreme top, right portion of the diagram and have the highest shock resistance among ceramics over the full range of heat transfer coefficient. It is also clear from the figure that the relative order of merit can switch between competing materials, depending on the magnitude of Bi. For example, beryllium oxide, BeO, has a higher value of $k\sigma_f/E\alpha$ than alumina, Al_2O_3, and is preferable for applications of low heat transfer (small Bi). When surface heat transfer is high (large Bi), $\sigma_f/E\alpha$ becomes the relevant material parameter, and alumina has a superior shock resistance to BeO.

5.2. Merit indices for toughness-controlled failure

A similar strategy can be employed to rank materials on the basis of failure from a dominant crack by thermal shock. The toughness-based fracture criterion for hot and cold shock is taken to be that $K_{\max}(a^*, t^*)$ attains the fracture toughness of the solid K_{IC}. The maximum temperature jump sustainable by the solid ΔT in the extreme case of perfect heat transfer ($Bi = \infty$) follows from equations (14a) and (16a) as

$$\Delta T = A_3 \frac{K_{IC}}{E\alpha\sqrt{\pi H}} \tag{19}$$

where $A_3 \approx 4.5$ for cold shock, and $A_3 \approx 5.6$ for hot shock. The temperature jump sustainable increases with decreasing Biot number, so that in the limit of small Biot number ($Bi < 1$), ΔT follows from equations (14a) and (16a) as

$$\Delta T = A_4 \frac{K_{IC}}{E\alpha\sqrt{\pi H}} \frac{1}{Bi} \equiv A_4 \frac{K_{IC}}{E\alpha\sqrt{\pi H}} \frac{k}{hH} \tag{20}$$

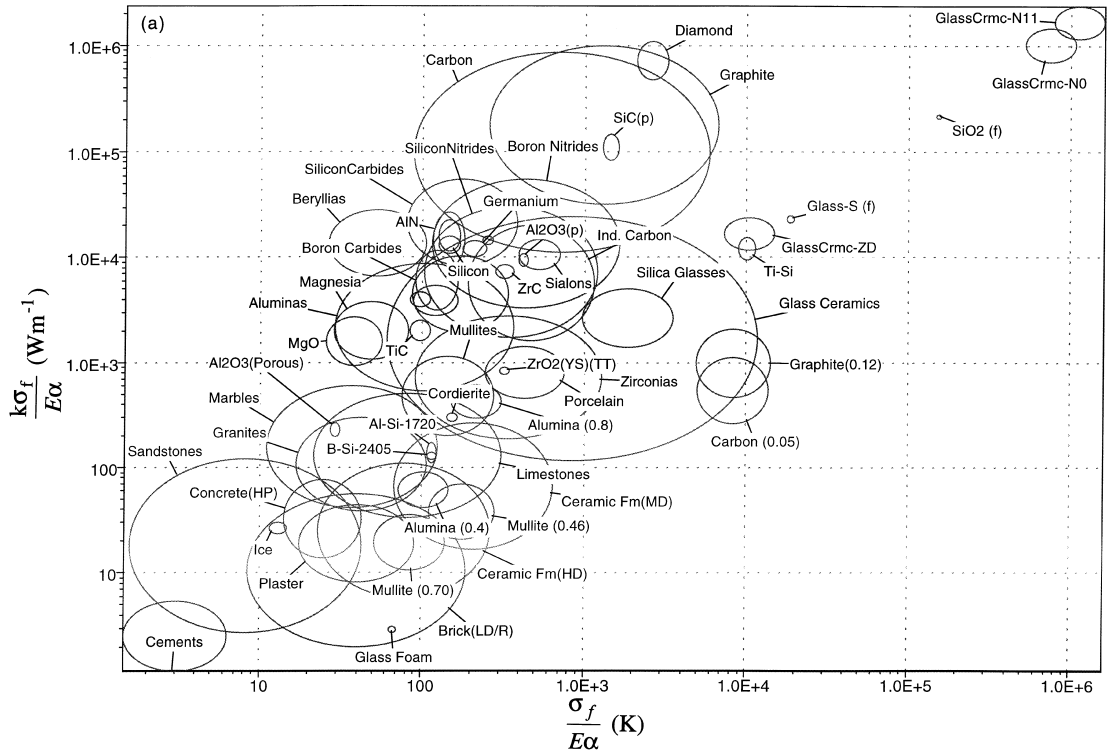

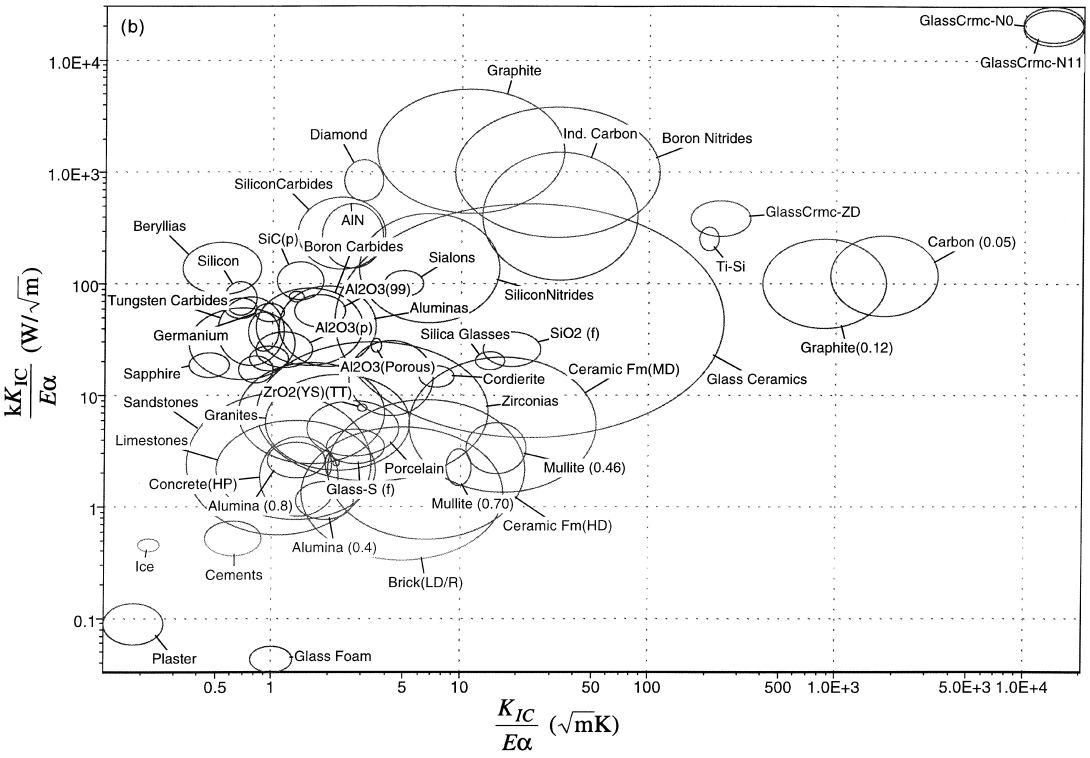

Figures 6(a) and (b). *Caption overleaf.*

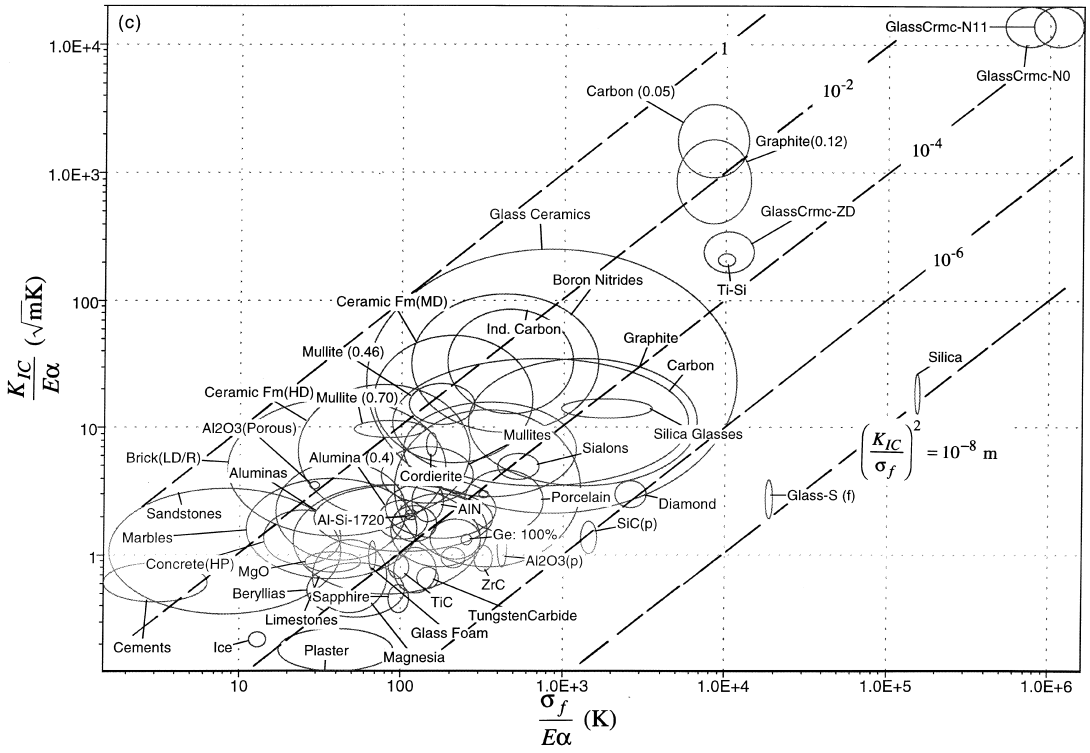

Fig. 6. (a) The merit indices for strength-controlled failure $k\sigma_f/E\alpha$ at low Bi values vs $\sigma_f/E\alpha$ at high Bi values, (b) merit indices for toughness-controlled failure $kK_{IC}/E\alpha$ vs $K_{IC}/E\alpha$, and (c) $K_{IC}/E\alpha$ vs $\sigma_f/E\alpha$, with the guide lines H_f added to help in selecting materials according to both strength- and toughness-based fracture criteria.

where $A_4 \approx 9.5$ for cold shock, and $A_4 \approx 12$ for hot shock.

From equations (19) and (20) it can be deduced that, for toughness-controlled thermal shock, the best candidate materials have a high value of $K_{IC}/E\alpha$ for ideal heat transfer ($Bi = \infty$), and a high value of $kK_{IC}/E\alpha$ for poor heat transfer ($Bi < 1$). A large number of engineering ceramics are displayed on a map with $kK_{IC}/E\alpha$ and $K_{IC}/E\alpha$ as axes, see Fig. 6(b). The relative location on the map is qualitatively similar to that given in Fig. 6(a) for strength-controlled thermal shock, and similar conclusions can be drawn from the map. For example, glass ceramics and graphites have the best thermal shock resistance amongst the ceramics. The relative order of merit depends somewhat on the Biot number: alumina has a superior shock resistance to beryllium oxide for ideal heat transfer, but is inferior for poor heat transfer.

There are two separate detrimental effects of increasing specimen size on thermal shock resistance, for both cold shock and hot shock. For toughness-controlled failure, dimensional considerations dictate that the thermal shock resistance decreases with increasing plate thickness $2H$, at all Biot numbers; this is clear from examination of equations (19) and (20). Further, when surface heat transfer is imperfect ($Bi < \infty$) the maximum temperature jump for both strength- and toughness-controlled failure decreases with increasing Biot number, see equations (18) and (20); thus, ΔT decreases with increasing H. Plate thickness has no effect on thermal shock resistance only for the case of strength-controlled failure with perfect heat transfer, see equation (17).

The issue of deciding whether a material selection procedure should be based on a strength criterion or a toughness criterion is a delicate one. It is instructive to plot data for engineering ceramics on a map for ideal heat transfer, with axes $K_{IC}/E\alpha$ and $\sigma_f/E\alpha$, as shown in Fig. 6(c). Ceramics with a high shock resistance from the strength viewpoint lie in the regime of large $\sigma_f/E\alpha$ value; and, ceramics with a high shock resistance from the toughness viewpoint lie in the regime of large $K_{IC}/E\alpha$ value. It is clear from the map that material data cluster along the leading diagonal: materials such as glass ceramics with a high $\sigma_f/E\alpha$ value also have a large $K_{IC}/E\alpha$ value. Equivalently, the ranking of materials by the strength criterion is the same as that given by the toughness criterion.

Dimensional analysis, and consideration of equations (17)–(20) reveal that the admissible temperature jump for both cold shock and hot shock is less for toughness-controlled fracture than for strength-controlled fracture, at a sufficiently large plate thickness. A transition plate thickness value H_t exists for which ΔT is equal for toughness-controlled failure and for strength-controlled failure. Consider first the case of ideal heat transfer, $Bi = \infty$. Then, upon equating the ΔT values for the strength criterion (17) and for the toughness criterion (19), it is found that

$$H_t \approx \left(\frac{K_{IC}}{\sigma_f}\right)^2 \tag{21}$$

for both cold and hot shock. In the other limit of poor heat transfer ($Bi < 1$), equating ΔT according to equations (18) and (20) gives

$$H_t \approx \left(\frac{K_{IC}}{\sigma_f}\right)^2 Bi \tag{22}$$

for both cold and hot shock. Lines of constant H_t according to definition (21) have been added to Fig. 6(c), and may be interpreted as follows. Materials which lie along a line of constant H_t have the same thermal shock resistance according to the strength criterion and to the toughness criterion, for a plate of thickness $2H_t$. For plates of this thickness, the strength-based criterion is conservative for materials lying above the line, and the toughness-based criterion is conservative for materials lying below the line. Materials with a large value of H_t can be considered to have high damage tolerance, compared with materials of low H_t value: thus, the H_t value can be thought of as a useful measure of damage tolerance.

6. CASE STUDY: THE POTENTIAL USE OF CERAMIC FOAMS FOR THERMAL SHOCK APPLICATIONS

At first sight, it is unclear whether a ceramic foam has a superior or inferior thermal shock resistance to that of a fully dense ceramic. The presence of porosity in a foam reduces its thermal conductivity, fracture toughness, failure stress, elastic modulus, and many other physical properties. The coefficient of thermal expansion and thermal diffusivity are generally not affected by porosity provided the pores contain gases and not liquids. In this section, the thermal shock resistance of a brittle foam is estimated compared to that of the solid material.

Consider, for illustration, the influence of porosity on the thermal shock fracture resistance of an insulation plate made of ceramic foam. On writing ρ^* for the density of the foam, and ρ_s for the density of the cell wall material, the relative density can be expressed as ρ^*/ρ_s and, to first order, dictates the properties of the foam. For simplicity, it is assumed that the foam consists of open cells and the surfaces of the foam plate are insulated to prevent the penetration of convective medium into the foam cells. The elastic modulus of the foam E^* derives mainly from the bending of struts making the cell edges, and is given approximately by [22]

$$E^* = E_s(\rho^*/\rho_s)^2. \tag{23}$$

Here and below, the superscript "*" is used to denote foam properties and the subscript "s" for properties of the solid material of which the foam is made. According to Gibbon and Ashby [22], the strength of the foam in compression σ_f^* is related to the cell wall strength σ_{fs} by

$$\sigma_f^* = 0.2\sigma_{fs}\left(\frac{\rho^*}{\rho_s}\right)^{3/2}. \tag{24}$$

The fracture toughness of the foam scales with the relative density, cell size l and fracture strength of the cell wall material according to

$$K_{IC}^* = 0.65(\rho^*/\rho_s)^{3/2}\sigma_{fs}\sqrt{\pi l}. \tag{25}$$

It is convenient to relate the tensile strength of the cell wall material σ_{fs} to the fracture toughness K_{IC}^s and the intrinsic flaw size a of the cell wall material

$$\sigma_{fs} = \frac{K_{IC}^s}{\sqrt{\pi a}} \tag{26}$$

and thereby write the fracture toughness of the foam as

$$K_{IC}^* = 0.65(\rho^*/\rho_s)^{3/2}K_{IC}^s\sqrt{l/a}. \tag{27}$$

This expression is physically meaningful only for the case $l \gg a$: it is assumed that flaws within the cell wall material are on a much smaller length scale than the cell size.

The thermal expansion coefficient for the foam is taken to be equal that of the cell wall material, and the thermal conductivity of the foam is taken as

$$k^* = (2/3)k_s(\rho^*/\rho_s). \tag{28}$$

Here, the relatively small contributions from gaseous conduction and thermal radiation have been neglected [22].

To proceed, the estimated thermal shock resistance of the foam ΔT^* is compared to that of the cell wall material ΔT_s from equations (17) and (18) for crush strength-controlled failure, and from equations (19) and (20) for toughness-controlled failure. Then, for both cold shock and hot shock, it is found that

$$\frac{\Delta T^*}{\Delta T_s} = 0.2\left(\frac{\rho^*}{\rho_s}\right)^{-1/2} \tag{29}$$

for ideal heat transfer, crush strength-based failure

$$\frac{\Delta T^*}{\Delta T_s} = 0.133\left(\frac{\rho^*}{\rho_s}\right)^{1/2} \tag{30}$$

for $Bi < 1$, crush strength-based failure

$$\frac{\Delta T^*}{\Delta T_s} = 0.65\left(\frac{\rho^*}{\rho_s}\right)^{-1/2}\sqrt{\frac{l}{a}} \tag{31}$$

for ideal heat transfer, toughness-based failure, and

$$\frac{\Delta T^*}{\Delta T_s} = 0.43\left(\frac{\rho^*}{\rho_s}\right)^{1/2}\sqrt{\frac{l}{a}} \tag{32}$$

for $Bi < 1$, toughness-based failure.

For the sake of argument take $l = 10a$ in equations (31) and (32). (Note that the precise value of l/a has only a moderate effect on the expression for $\Delta T^*/\Delta T_s$ due to the square root dependence on l/a.) Typically, the relative density of ceramic foams is in the range 0.03–0.3, and equations (30) and (32) suggest that foams are inferior to their fully dense parent materials, at low Biot numbers, due mainly to their poor conductivities. However, in the case of high surface heat transfer, equation (29) reveals that foams have a higher shock resistance than the parent solid for $\rho^*/\rho_s < 0.04$, based on the crush strength criterion. In similar fashion, for high surface heat transfer, equation (31) reveals that foams have a higher shock resistance than the parent solid for all ρ^*/ρ_s less than unity, based on the toughness criterion. In conclusion, at large Bi numbers, open-cell foams have promise for improved thermal shock resistance, provided the relative density is sufficiently low. Indeed, from Figs 6(a) and (b), it can be seen that graphite and zirconia (ZrO_2) foams, among others, lie to the right of their respective parent solid materials.

If, during thermal shocking, the convective medium can infiltrate into the interior structure of open-celled brittle foams, the situation is more complicated due to the coupling of global thermal stress and the thermal stress induced at the strut level. A preliminary study of thermal shock damage under such conditions can be found in Orenstein and Green [23].

7. APPLICATION TO THERMAL FATIGUE

The results of the current study can also be used to estimate the thermal fatigue resistance of ceramics, metals and polymers. Repeated thermal shock of a plate can lead to the initiation and growth of fatigue cracks. A conservative approach is to design for infinite fatigue life, and to consider two failure criteria:

(i) A stress-based criterion for the *initiation* of fatigue cracks. It is assumed that cracks do not initiate when σ_{max} for each thermal shock is less than the endurance limit of the material σ_e; here, σ_e is defined as the stress amplitude at a fatigue life of 10^7 cycles in a fully reversed fatigue test.

(ii) A stress-intensity based criterion for the *propagation* of an existing crack. It is assumed that a thermally-shocked plate has infinite crack growth life provided the stress intensity K_{max} for each thermal shock is less than the fatigue threshold ΔK_{th} of the material. Here, the fatigue threshold is defined as the value of the cyclic stress intensity, ΔK, corresponding to a crack growth rate of 10^{-10} m/cycle, in a test for which the minimum load of each cycle equals zero.

The merit indices for stress-controlled fatigue crack initiation are $k\sigma_e/E\alpha$ for $Bi < 1$ and $\sigma_e/E\alpha$ for ideal heat transfer $Bi = \infty$. Alternatively, when the plate contains cracks on the length scale of its thickness, the pertinent merit indices become $k\Delta K_{th}/E\alpha$ and $\Delta K_{th}/E\alpha$ for $Bi < 1$ and $Bi = \infty$, respectively.

It is instructive to compare the thermal fatigue properties for a range of ceramics, metals, and polymers with their thermal shock resistance, for the case of ideal heat transfer, see Figs 7(a) and (b). The data are taken primarily from the Cambridge Materials Selector [21] and from Fleck *et al.* [24]. Figure 7(a) takes as axes the thermal shock merit indices $\sigma_f/E\alpha$ and $K_{IC}/E\alpha$, and Fig. 7(b) adopts the equivalent parameters $\sigma_e/E\alpha$ and $\Delta K_{th}/E\alpha$. The particular choice of materials is such as to define the outer boundaries of material behaviour for the generic classes of solid: ceramics, metals and polymers. Consider first Fig. 7(a). It is noted that the high fracture toughness exhibited by metals affords them a high thermal shock resistance for the case of a pre-cracked plate. When strength is the dominant failure criterion, certain ceramics (such glass ceramics, graphites and silica glass) out perform the metals. It is notable that the field of ceramics covers a wide range, which partly explains the need for careful materials selection for thermal shock applications. Polymers have a relatively low Young's modulus, and thereby a reasonable thermal shock resistance: they lie between the data for metals and ceramics. Now consider the thermal fatigue response, as shown in Fig. 7(b). The field for metals moves downwards by about an order of magnitude as the fatigue limit for metals is about an order of magnitude less than their fracture toughness. The drop in strength property from σ_f to σ_e is less: about a factor of two. Thus, metals have a significantly worse thermal fatigue performance compared to their behaviour under a single thermal shock. In contrast, for polymers and ceramics, there is only a

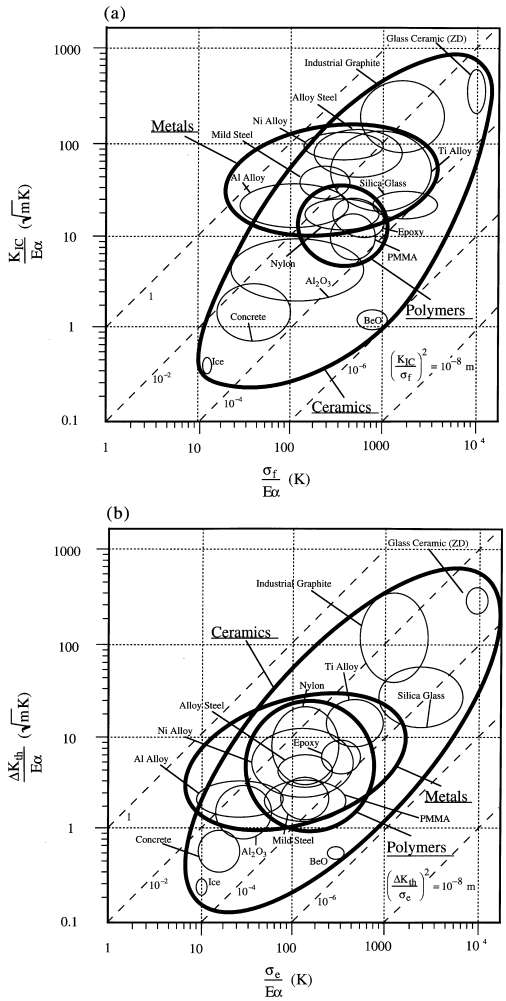

Fig. 7. At high values of *Bi*, the materials selection chart of (a) $K_{IC}/E\alpha$ vs $\sigma_f/E\alpha$ for a single thermal shock, (b) $\Delta K_{th}/E\alpha$ vs $\sigma_e/E\alpha$ for repeated thermal shocks. The guide lines H_t help in selecting materials according to both strength- and toughness-based fracture criteria, for stable and for cyclic thermal loading.

small drop in values of $\sigma_e/E\alpha$ and $\Delta K_{th}/E\alpha$ compared with the static properties $\sigma_f/E\alpha$ and $K_{IC}/E\alpha$, respectively. It is clear from Fig. 7(b) that the field for metals lies within that for ceramics: there is little advantage in using metals for thermal fatigue applications in preference to ceramics, unless other factors dominate (such as cost and manufacturability). For completeness, the transition plate thickness H_t is defined for the fatigue case in a similar manner to that given in equation (21)

$$H_t \approx \left(\frac{\Delta K_{th}}{\sigma_e}\right)^2. \tag{33}$$

Contours of H_t are included for the fatigue case in Fig. 7(b), and for the static case in Fig. 7(a) making use of equation (21). It is noted that the values of H_t are consistently smaller for fatigue loading than for static loading: the materials are less damage-tolerant under fatigue loading than under static loading.

Acknowledgements—The authors are grateful to W. J. Clegg and M. F. Ashby for insightful discussions.

REFERENCES

1. Manson, S. S. and Smith, R. W., *Trans. ASME*, 1956, **78**, 533.
2. Kingery, W. D., *Property Measurements at High Temperatures*. Wiley, New York, 1959.
3. Hasselman, D. P. H., *J. Am. Ceram. Soc.*, 1969, **52**, 600.
4. Baron, H. G., Thermal shock and thermal fatigue, in *Thermal Stresses*, ed. P. P. Benham *et al.* Pitman, London, 1964.
5. Manson, S. S., *Thermal Stress and Low-Cycle Fatigue*. McGraw-Hill, New York, 1966.
6. Hasselman, D. P. H., *Ceram. Bull.*, 1970, **49**, 1033.
7. Evans, A. G., *Proc. Br. Ceram. Soc.*, 1975, **25**, 217.
8. Nied, H. F., *J. Therm. Stresses*, 1983, **6**, 217.
9. Rizk, A. E.-F. A. and Radwan, S. F., *J. Therm. Stresses*, 1993, **16**, 79.
10. Jin, Z.-H. and Mai, Y.-W., *J. Am. Ceram. Soc.*, 1995, **78**, 1873.
11. Emery, A. F., Walker, G. E. Jr and Williams, J. A., *Trans. ASME J. Basic Engng*, 1969, **91**, 618.
12. Carslaw, H. S. and Jaeger, J. C., *Conduction of Heat in Solids*. Oxford University Press, Oxford, 1959.
13. Nied, H. F., *Engng Fract. Mech.*, 1987, **26**, 239.
14. Manson, S. S., Behaviour of materials under conditions of thermal stress, *Nat. Advis. Commun. Aeromaut. Rep.*, 1954, No. 1, 170.
15. Buessem, W., The ring test and its application to thermal shock problem. Metallurgy Group, Office of Air Research, Wright-Patterson Air Force Base, Dayton, Ohio, 1950.
16. Hutchinson, J. W. and Suo, Z., *Adv. appl. Mech.*, 1992, **29**, 63.
17. Lu, T. J., *J. Am. Ceram. Soc.*, 1996, **79**, 266.
18. Cotterell, B. and Rice, J. R., *Int. J. Fract.*, 1980, **16**, 155.
19. Prakash, O., Sarkar, P. and Nicholson, P. S., *J. Am. Ceram. Soc.*, 1995, **78**, 1125.
20. Tu, W.-C., Lange, F. F. and Evans, A. G., *J. Am. Ceram. Soc.*, 1996, **79**, 417.
21. Cambridge Materials Selector, Granta Design Ltd, Cambridge, U.K.
22. Gibbon, L. J. and Ashby, M. F., *Cellular Solids: Structures and Properties*, 2nd edn. Cambridge University Press, Cambridge, 1997.
23. Orenstein, R. M. and Green, D. J., *J. Am. Ceram. Soc.*, 1992, **75**, 1899.
24. Fleck, N. A., Kang, K. J. and Ashby, M. F., *Acta mater.*, 1994, **42**, 365.
25. Tada, H., Paris, P. C. and Irwin, G. R., *Stress Analysis of Cracks Handbook*. Del Research, St. Louis, Missouri, 1985.

APPENDIX OVERLEAF

APPENDIX A

Definition of Green's function $F_1(z/H,a/H)$ in equation (12)

The dimensionless function $F_1(z/H,a/H)$ appearing in equation (12) is given by [25]

$$F_1\left(\frac{z}{H},\frac{a}{H}\right)=f_1\left(\frac{a}{H}\right)+f_2\left(\frac{a}{H}\right)\left(\frac{H-z}{a}\right)+f_3\left(\frac{a}{H}\right)\left(\frac{H-z}{a}\right)^2+f_4\left(\frac{a}{H}\right)\left(\frac{H-z}{a}\right)^3 \tag{A1}$$

where

$$f_1\left(\frac{a}{H}\right)=0.46+3.06\left(\frac{a}{2H}\right)+0.84\left(1-\frac{a}{2H}\right)^5+0.66\left(\frac{a}{2H}\right)^2\left(1-\frac{a}{2H}\right)^2$$

$$f_2\left(\frac{a}{H}\right)=-3.52\left(\frac{a}{2H}\right)^2$$

$$f_3\left(\frac{a}{H}\right)=6.17-28.22\left(\frac{a}{2H}\right)+34.54\left(\frac{a}{2H}\right)^2-14.39\left(\frac{a}{2H}\right)^3-\left(1-\frac{a}{2H}\right)^{1.5}-5.88\left(1-\frac{a}{2H}\right)^5-2.64\left(\frac{a}{2H}\right)^2\left(1-\frac{a}{2H}\right)^2$$

$$f_4\left(\frac{a}{H}\right)=-6.63+25.16\left(\frac{a}{2H}\right)-31.04\left(\frac{a}{2H}\right)^2+14.41\left(1-\frac{a}{2H}\right)^5+2\left(1-\frac{a}{2H}\right)^{1.5}+5.04\left(1-\frac{a}{2H}\right)^5+1.98\left(\frac{a}{2H}\right)^2\left(1-\frac{a}{2H}\right)^2.$$

Definition of Green's function $F_2(z/H,a/H)$ in equation (15)

The dimensionless function $F_2(z/H,a/H)$ appearing in equation (15) is given by [25]

$$F_2(z/H,a/H)=1+\left(\frac{\pi}{\sqrt{\pi^2-4}}-1\right)\left(1-\cos\frac{\pi a}{2H}\right)\sqrt{1-\left(\frac{z}{H}\right)^2}. \tag{A2}$$